Engineering Structures 302 (2024) 117427

Contents lists available at ScienceDirect

Engineering Structures

journal homepage: www.elsevier.com/locate/engstruct

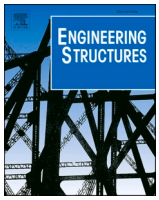

Shear strength of an anchor post-installed into a hardened concrete member

Paolo Foraboschi

Università IUAV di Venezia – Dipartimento Culture del Progetto, Dorsoduro 2206, 30123 Venice, Italy

A R T I C L E I N F O

Keywords:
Adhesive anchor
Hardened concrete anchor
Injection anchor
Mechanical expansion anchor
Straight shaft connector

A B S T R A C T

Literature has recently provided the analytical model that predicts the shear strength of the anchor embedded into masonry. It is apparent that this model does not apply to the anchor embedded into concrete, as the ultimate contact pressures are different. A gap in the literature was hence filled, but there existed a remaining gap. In order to fill that last gap, further research was done. This paper is herein an account of that work. The paper deals with the anchor post-installed by drilling into an already compact concrete structure, used to transmit applied loads from an attachment to the concrete, subjected to a force acting at the end that emerges from the concrete and orthogonal to the anchor (shear force with no axial force), with large clearance from the edges, either alone or with large clearance from other anchors. Being post-installed, the embedded part of the anchor is a straight shaft with no hook at the embedded end, and with no nuts, washers, or plates attached to the shaft. The paper presents an analytical model absent in literature prior to this study that predicts the maximum shear force the anchor can carry, thus called "shear strength" of the anchor. The assumptions of the analytical model were established from the results of a non-linear numerical model specifically constructed by the author. The predictive capacity of the analytical model and accuracy of its results were assessed and verified by experimental tests of real anchorages specifically designed and performed by the author. This paper also presents the numerical model and the comparisons of the analytical predictions to those experimental results, as well as comparisons to experimental results borrowed from literature and code provisions.

1. Introduction: subject matter and specific advancement over the present state of the art

The present paper focuses on the connector consisting in a straight shaft – called "anchor" – post-installed into hardened concrete, used to transmit applied loads from a structure – called "attachment" – to an existing concrete structure. One end of the anchor is embedded into the concrete while the other end protrudes from the concrete surface and is subjected to a transverse force, i.e., a force orthogonal to the anchor. That force is called "shear force" and is denoted by V (hence the anchor is given the name "shear anchor"). The term "shear force" refers to the external force applied to the anchor, while the internal forces in the anchor induced by the shear force are internal bending moment and internal shear force (but no or marginal internal axial force). The anchor is far from the edges and other anchors, and its shaft is strong (Section 2).

As detailed in Section 3, which provides the background and the state of the art, this issue constitutes a gap in scientific and technical literature. The same anchor but embedded into masonry was the subject of a recently published paper [1], which has presented a two-step analytical model. The first step provides the ultimate contact pressures, and the second step of that model predicts the shear strength of the masonry shear anchor. Needless to say, [1] does not apply to the shear anchor embedded into concrete because the mechanism that resists the contact pressures between anchor and concrete is different, and consequently the ultimate contact pressures are different.

Recent literature also includes the mathematical model of the anchor group post-installed in concrete [2]. That analytical model predicts the anchor group effect on the shear anchor, while it applies neither to the single anchor (individual anchor) nor to the anchor groups with sufficient spacing between the anchors (anchor groups whose strength is not governed by the group effect, i.e., whose shear strength does not depend on anchor spacing).

In order to fill that gap and completely resolve the issue of the shear anchor, the author carried out a similar research activity devoted to analyzing the shear anchor post-installed into concrete, which is either single or part of a group whose strength is the sum of the strengths of each single anchor (i.e., the strength of the group does not depend on the spacing of the anchors). This paper reports that activity. In the hope that this effort will be useful to the research, profession, and industry, the

E-mail address: paofor@iuav.it.

https://doi.org/10.1016/j.engstruct.2023.117427
Received 3 September 2023; Received in revised form 25 November 2023; Accepted 21 December 2023
Available online 11 January 2024

author presents here an analytical, closed-form model that predicts the shear strength of an anchor post-installed into hardened concrete. The anchor's shear strength, which is the ultimate value of V, is denoted by V_u.

An anchor post-installed into an existing structure is different than an anchor cast in a new structure, being the latter placed before pouring the concrete while the former inserted into hardened concrete. The embedded end of an anchor that is installed before pouring the concrete often is hooked, and the embedded part of the shaft typically includes nuts, washers, and/or plates. Moreover, the concrete includes specific bars and stirrups that improve the anchoring capacity of the concrete. Those devices largely strengthen the shear strength of the anchor. Conversely, the post-installed anchor is a straight shaft (rectilinear shank) with no strengthening devices along it. Moreover, no bars and stirrups embrace the anchor, as the reinforced concrete structure had not been designed to bear an anchor.

Accordingly, this paper uses the term "concrete" although the members are usually made of reinforced concrete, because the members do not include any bar or stirrup specifically placed to strengthen the capacity of the concrete to bear the anchor.

The attachment that is considered in this research work induces no more than marginal axial force in the anchor (negligible tensile force), as detailed in Section 2, and plays no role in the ultimate behavior of the anchor.

This paper directly refers to anchors made of steel, but it encompasses any anchor stronger and stiffer than the surrounding concrete.

Metal anchors can be divided into two types: adhesive anchors and mechanical anchors. The model that has been constructed does not make any differences between the types of anchors, as the anchor that is considered is subjected to shear force and no more than small axial force. Thus, the pull-out mechanism (extraction force) is not involved, and the bond consists only in the contact between concrete and embedded system (the embedded system is the anchor plus, in the case of adhesive anchor, the anchoring material).

The whole fastening system is called "anchorage". The anchorage is hence composed of anchor, drilled hole, concrete that surrounds the drilled hole, and anchoring material in the case of adhesive anchor.

2. Strength hierarchy and requirements

The anchorage that this paper focuses on satisfies a strength hierarchy criterion according to which the embedded system is the strongest component, while the concrete that surrounds the drilled hole is the weakest component, so that the failure of the anchorage is dictated by the surrounding concrete. That strength hierarchy is not a restriction or an assumption of the model but a necessary condition for a design to be optimal and a job well executed.

This paper is devoted to the anchor with sufficient clearance from the edges of the concrete structure it is embedded into, and from other anchors in the case of anchor group, so that the shear strength does not depend on those clearances.

The respect of the strength hierarchy shall be checked at the end of the assessment process by verifying that the steel-governed shear strength, edge-governed shear strength, and group-governed shear strength, which can be predicted by using models borrowed from literature or numerical models, are greater than the concrete-governed shear strength predicted by the analytical model presented in this paper.

Furthermore, the anchor must be subjected to no more than moderate tensile axial force. If the axial force is more than moderate, in fact, then the prediction of this model overrates the actual shear strength of the anchor because there is a significant interaction between shear force and axial force. More specifically, if the axial force is no more than moderate, that interaction is negligible. If conversely the axial force is greater, the interaction substantially reduces the shear strength. Again, that is not a restriction or an assumption of the model but a necessary condition in order to take full advantage of the potential of the anchor and concrete.

For that reason, the shear force applied to an anchor group should have no more than moderate eccentricity with respect to the concrete surface. In fact, such eccentricity induces bending moment acting on the whole group, which in turn gives rise to a couple composed of a compressive force and a tensile force. The compressive force results in compressive contact pressures acting onto the concrete surface, while the tensile force introduces internal tensile axial forces in some anchors. While those compressive contact pressures play no role in anchor's shear strength, the internal tensile axial force in an anchor gives rise to the above-mentioned interaction, which may cause a decrease in the shear strength. For that reason, moreover, the connection between the attachment and the anchor group must be a hinge.

Differently than for the anchor group, for the single anchor the eccentricity of the shear force does not give rise to any axial force, because this eccentricity induces a bending moment that acts on the single anchor, which is resisted in the same way as the shear force. Nevertheless, this eccentricity reduces the shear strength as well. So, the eccentricity of the shear force applied to an anchor, on one hand, is accounted for by this model, but on the other hand, should be as small as possible.

The anchor is (the anchors are) usually collected by a plate, which is adherent to the concrete surface and is connected to the attachment. That plate, which usually is made of steel, provides the anchor with some extra strength because it restrains the rotation of the anchor's external end. Nevertheless, that supplementary strength is often small, as proven in [1] for the masonry shear anchor and confirmed in this research work for the concrete shear anchor. Thus, that extra strength is here neglected, which is a simplifying and conservative assumption. Modeling ignores hence that plate and considers the anchor as independent of the attachment. Accordingly, the external end of the anchor is assumed to be free, and the shear force is directly applied to it.

The anchor must be installed in uncracked concrete; a strip of concrete around the anchor and parallel to the shear force must be uncracked (i.e., the anchor must be post-installed by drilling in an uncracked portion of concrete). However, that strip has not to be large, as proven by the tests presented in the following.

In brief, this paper is devoted to analyzing any post-installed anchor (i.e., installed into hardened concrete), however installed and bonded, subjected to a shear force V acting at the end protruding from the concrete surface and no more than marginal axial force, with large edge distance, and (in the case of anchor group) with large anchor spacing. The shear strength is hence dictated by the concrete that surrounds the anchor, while it depends neither on the distance from the edges, nor on the spacing of the anchors, and nor even on the strength of the materials that compose the embedded system.

3. Gaping absence in literature about the shear anchor

This section presents an overview of the previously published papers on concrete anchors and refers to some academic articles, with the double aim of showing the gap identified in the Introduction and providing key sources on the topic.

Anchor embedded into concrete has been the subject matter of many papers. The vast majority of them deals with cast-in anchors (some mainstream papers are [3–12]), while post-installed anchors are dealt with by the minor part of them (e.g., [13–20]). Moreover, this minor part mainly deals with pull-out strength, combined shear force and axial tensile force, and cyclic or seismic loadings [21–24]. As a result, the pure shear behavior of anchors post-installed into hardened concrete (embedded in existing structures) and subjected to static (monotonic) loadings is dealt with by a relatively small number of papers.

In addition, almost all those papers investigate the strength dictated by the distance of the anchor from the edges (edge effect) [25–29], group effect (anchor group spacing) [2,30–33], and dowel action (strength dictated by the metal of the anchor's shaft) [11,21,34–36]. Conversely, the strength of an anchor whose clearance from the edges is

large (no edge effect), whose spacing between the adjacent anchors is large (no anchor group effect), and whose shaft is strong (no dowel action failure mechanism) is dealt with by a relatively slight number of papers. So, only a small amount of literature covers the subject of anchors whose strength is dictated by the surrounding concrete.

Another lack of balance in the literature that must be highlighted is that most of the papers about anchors present experimental research works [3,9,11,20,22,24–28,31–34,37–51], empirical formulations [4,10,13,14,20,26,33,40,44,45,52–57], and numerical analyses [3,32,35,36,58–65], while only a small minority of the published papers present analytical models. And again, the papers that present analytical models not only are a minor fraction of the literature about anchors, but also are devoted to analyzing the failure modes dictated by clearance from the edges [8,39,66], anchor spacing [2,30,67], or steel (metal) failure [11,35], but not by the concrete that surrounds the anchor. Other literature sources about anchor's analytical modeling are [68], which provides a comprehensive literature review, [41], which describes four types of available expansion concrete anchors (i.e., anchors that transfer loads to the concrete by expanding laterally against the sides of a drilled hole) and includes some information about modeling, and [1,69–71], which provide analytical models of the masonry anchor under different loading conditions.

Ultimately, literature does not provide any analytical model to predict the shear strength of a post-installed concrete anchor that is sufficiently far from the edges and from the other anchors (anchor group), with a sufficiently strong shaft. This is not to be considered a criticism about published work. The true fact is that this subject matter has simply not been tackled yet. In actuality, the research work presented in this paper has been carried out to fill that gap.

This activity is part of a comprehensive research program composed of two other activities, which were devoted to addressing the masonry shear anchor [1] and the concrete anchor group [2], respectively. The former has filled the analogous gap for masonry structures, while the latter for close- spaced anchors.

The concrete anchor is also dealt with by many codes, standards, reports, and test methods edited by organizations for technical assessment and by technical committees [72–83]. However, the technical literature follows the scientific literature [84,85]. Accordingly, those documents mainly focus on cast-in anchors, pull-out strength, combined tension and shear, concrete edge failure, anchor group effect, and anchor's shaft failure. Moreover, those documents only present empirical formulas and testing methods. Conversely post-installed anchors, shear strength dictated by the concrete that surrounds the anchor, and analytical modeling have received much less attention in the technical literature.

Ultimately, the above account of what has been published on the topic has shown that neither the scientific literature nor the technical literature has tackled the post-installed anchor that has both sufficiently large diameter and sufficiently long embedded length, and that is sufficiently far from both the edges and other anchors. Furthermore, upon closer inspection, the above literature review has proven that a straight shaft anchor embedded into concrete, with no nut, washer, or plate along the embedded shaft can be analyzed for shear only empirically but not analytically.

Evidence of what has been stated above can be inferred by analyzing a popular document [73], i.e., Appendix B ("Anchoring to concrete") of ACI Committee 349. The formulation presented in that document is empirical. As such, it has no theoretical justification. Section 11 of this paper shows that [73] gives good estimates only for anchorages both similar to those used to calibrate the formulas (medium diameters) and whose failure is not dictated by the surrounding concrete. On the contrary, [73] drastically underestimates the shear strength of small diameters and drastically overestimates the shear strength for large diameters, and above all, drastically misestimates the shear strength of the anchors whose failure is dictated by the crushing of the surrounding concrete. The flaw stemming from small and large diameters, which is due to the empirical nature of the formulation, is something that both researchers and practitioners are already very well aware of and has also been pointed out previously in literature [84]. The flaw stemming from concrete crushing failure mode, which is due to a formulation that ignores the contact pressures, has not been pointed out before, although ignoring it can lead to unsafe predictions.

The above considerations are also confirmed by another popular document [74], i.e., ACI Committee 318–19. An excerpt from Chapter 17 (*Anchoring to concrete*) of [74] (which more or less is equal to the previous ACI 318–14) prescribes: *"For post-installed anchors where sleeves extend through the shear plane, V_{sa}* (Ed. V_{sa} = shear strength) *shall be based on the 5% fractile of results of tests performed and evaluated in accordance with ACI 355.2. Alternatively, Eq. (17.7.1.2b) shall be permitted to be used."* The provisions of [74] are hence either an empirical formula or a testing program, while no analytical formula is provided. But, above all, not even [74] encompasses anchor's shear strength dictated by the surrounding concrete. Section 11 of this paper shows that these provisions, which are almost equal to those of [73], are largely inaccurate.

Producers and manufactures have attempted to provide practitioners with plain tools, by publishing reports and instructions, and making software programs available that allow for the implementation of their formulations. Regrettably, that activity has not attempted to fill the gap that has not been addressed by literature. As a result, the predictions of those formulations and that software can be either excessively conservative or totally unsafe. The first case occurs for the anchors with a small clearance from the edges or from other anchors, or having a weak shaft, due to the empirical nature of those formulations. In fact, the experimental data exhibits a very large dispersion, which implies that the 5% fractile is drastically lower than the mean value (0.50 fractile). The second case occurs for the anchors whose shear strength is dictated by the surrounding concrete, due to crushing. In fact, those formulations and those software programs ignore the actual failure mode of the anchor whose shaft is sufficiently strong and whose clearances from the edges and other anchors are sufficient.

That gap in scientific and technical literature implies that the shear strength of a post-installed concrete anchor cannot be predicted at the design stage but must be measured on-site by tests at the construction stage. Indeed, the only topic related to concrete anchors that is broadly covered by the scientific literature is the definition of testing procedures [7,10,11,13,14,26,31,35,50,68,70–85], and the only topic sufficiently covered by codes and recommendations is the standardization of methods to test anchors for use in concrete [72–82].

4. General reference system and nomenclature

The reference structure is an anchor embedded into a semi-space (half-space). The half-space is the concrete, the surface of the half-space is the outer face of the concrete, and the complementary half-space is the air. The diagram of the reference structure is shown in Fig. 1.

It should be anticipated right away that the model presented in this paper introduces two different semi-spaces (half-spaces). The first one is that of Fig. 1, while the second one is presented in the following.

In the case of adhesive anchor, the schematic includes the anchoring material. In fact, the anchoring material and the interface between anchor and anchoring material play no role in the ultimate behavior. Thus, modeling considers the whole embedded system without any differentiation.

The diameter of the drilled hole is denoted by ϕ (Fig. 2) and the diameter of the anchor by Ω (Fig. 1). Thus, $\phi - \Omega$ is the space between anchor and surrounding concrete (gap), which in the case of adhesive anchor is occupied by the anchoring material while in the case of mechanical anchor is zero ($\phi = \Omega$).

The length of the anchor is denoted by L (Fig. 1). The external end of the anchor protrudes from the concrete surface and is connected to the attachment, while the internal end is embedded in the concrete.

The external end of the anchor is either collected by a (steel) plate or

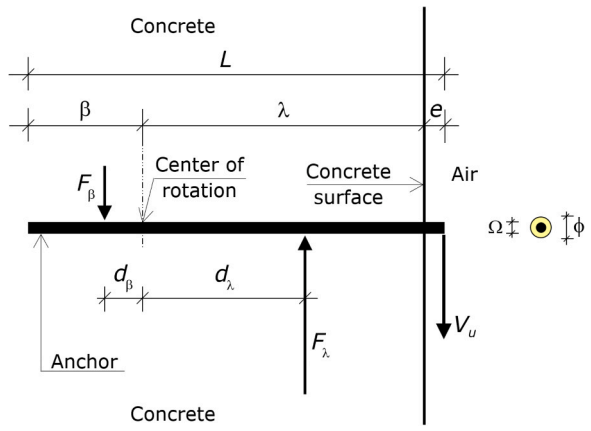

Fig. 1. Reference structure, with the forces acting at ultimate on the embedded system, including their application point and their distance from the rotation center. The transverse cross-section on the right refers to the adhesive anchor.

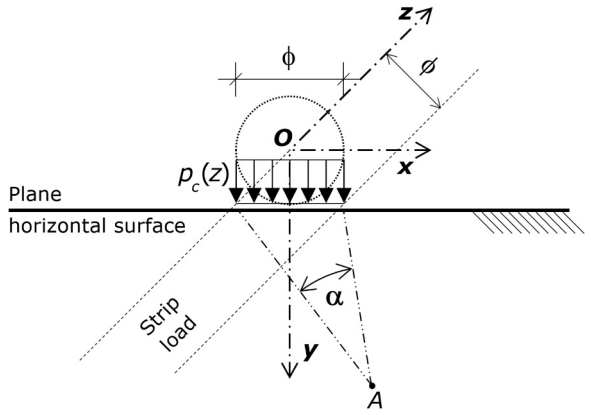

Fig. 2. Cartesian coordinate system *x*-*y*-*z* with origin *O*, and α-coordinate system of a generic point *A*. Contact pressures p_c at the coordinate *z*.

embedded into a concrete or timber component of the attachment. That connection restrains the rotation of the external end. As such, the connection provides the anchor's shear strength with a resisting contribution. As anticipated in Section 2, both this research and [1] have proven that this extra strength is no more than moderate. For the sake of simplicity, thus, that extra strength is herein neglected, which is a sufficiently accurate and safe assumption. Accordingly, the shear force *V* is applied at the anchor's external end, which is assumed to be free (Fig. 1), i.e., no bending moment is applied at the external end.

The distance of the external end from the concrete surface is denoted by *e* (Fig. 1). The embedded length of the anchor is hence $L - e$. Thus, the shear force *V*, which is applied at the external end, is eccentric by *e* to the concrete surface.

The positions in the space are described using a right-handed Cartesian coordinate system whose origin is on the surface of the half-space (i.e., on the outer face of the concrete), at the center of the anchor. The *x*-axis and *y*-axis lie on the surface. The *z*-axis is in the depth direction, and its positive direction is from the surface to inwards (Fig. 2).

The positions in the *x*-*y* plane are identified by the coordinate α along with the segment ϕ (Fig. 2). That coordinate system is alternative to the Cartesian coordinate system. For a given *z*, the coordinate α of a point *A* is the angle between two radii from *A* that pass through the edges of the segment of length ϕ, parallel to the *x*-axis, tangent to the drilled hole, and symmetric to the *y*-axis. A given α does not identify a single point of the *x*-*y* plane (aside from $\alpha = \pi$), but a plane curve. That coordinate system allows the diameter ϕ of the drilled hole to be eliminated.

5. Numerical modeling of the shear anchor embedded into concrete

The author constructed a non-linear numerical model that allowed the ultimate behavior of a concrete anchor to be simulated. The embedded system – anchor and anchoring material – was modeled as elastic, using the relevant elasticity moduli. The interface between anchor and anchoring material was modeled as a bilateral contact (adhesive anchor). The interface between uncracked surrounding concrete and embedded system was modeled as a bilateral contact in the case of adhesive anchors and as a unilateral contact in the chase of mechanical anchor. The interface between cracked surrounding concrete and embedded system was modeled as a unilateral contact.

The concrete in compression was modeled with the following constitutive law:

$$\sigma_c = \frac{\frac{E_c}{E_{c1}}\frac{\varepsilon_c}{\varepsilon_{c1}} - \frac{\varepsilon_c^2}{\varepsilon_{c1}^2}}{1 + \left(\frac{E_c}{E_{c1}} - 2\right)\frac{\varepsilon_c}{\varepsilon_{c1}}} f_{cm} \tag{1}$$

where ε_c denotes the compressive strains and σ_c the compressive stresses. Compressive strains and stresses are assumed to be positive.

The stress f_{cm} of Eq. (1) is the concrete compressive strength (the uniaxial crushing strength of the concrete), expressed in N/mm^2, $\varepsilon_{c1} = 2.2‰$, $E_{c1} = f_{cm}/\varepsilon_{c1}$, and E_c is the tangent modulus given by Eq. (2), where E_c is expressed in N/mm^2.

$$E_c = 11026 \cdot f_{cm}^{0.3} \tag{2}$$

For $\sigma_c < 0.4 \cdot f_{cm}$ and $\varepsilon_c < \varepsilon_{c1}$ (ascending branch), the stresses calculated using the linear equation $\sigma_c = E_c \cdot \varepsilon_c$ differ no more than marginally from the stresses calculated using the non-linear Eq. (1). The strain $\varepsilon_L = 0.4 \cdot f_{cm}/E_c$ can thus be called "pseudo-elastic limit".

The descending part of Eq. (1) is valid for $\sigma_c / f_{cm} \leq 0.5$. The stress σ_c equal to $0.5 \cdot f_{cm}$ is denoted by $\sigma_{c\lambda}$ and the strain at $\sigma_{c\lambda}$ is denoted by $\varepsilon_{c\lambda}$. The strain $\varepsilon_{c\lambda}$ is provided by the following Eq. (3).

$$\varepsilon_{c\lambda} = \varepsilon_{c1} \cdot \left\{ \frac{1}{2} \cdot \left(\frac{1}{2} \cdot \frac{E_c}{E_{c1}} + 1 \right) + \sqrt{\left[\frac{1}{4} \cdot \left(\frac{1}{2} \cdot \frac{E_c}{E_{c1}} + 1 \right)^2 - \frac{1}{2} \right]} \right\} \tag{3}$$

For $\varepsilon_c > \varepsilon_{c\lambda}$ the descending branch of the $\sigma_c - \varepsilon_c$ relationship was described using the following Eq. (4):

$$\sigma_c = \frac{1}{f_{cm} \cdot \left[\left(\frac{\Psi}{\nu} - \frac{2}{\nu^2} \right) \cdot \left(\frac{\varepsilon_c}{\varepsilon_{c1}} \right)^2 + \left(\frac{4}{\lambda} - \Psi \right) \cdot \frac{\varepsilon_c}{\varepsilon_{c1}} \right]} \tag{4}$$

where

$$\Psi = \frac{4 \cdot \left[\nu^2 \cdot \left(\frac{E_c}{E_{c1}} - 2 \right) + 2 \cdot \nu - \frac{E_c}{E_{c1}} \right]}{\left[\nu \cdot \left(\frac{E_c}{E_{c1}} - 2 \right) + 1 \right]^2} \tag{5}$$

in which

$$\nu = \frac{\varepsilon_{c\lambda}}{\varepsilon_{c1}} \tag{6}$$

Eq. (4) can be used either with a concrete crushing strain, denoted by ε_{cu}, or without any limit on the concrete strain ε_c. The model results demonstrated that the shear strength of the anchor depends slightly on ε_{cu}, since the greater ε_{cu} the greater the resultants of the internal forces acting on the anchor but the lower their lever arm, and vice versa. Therefore, Eq. (4) was used without any concrete crushing strain.

The uncracked concrete subjected to tension was modeled using a

stress-strain constitutive law composed of a bilinear relationship having two ascending branches with decreasing slope.

The cracked concrete was modeled using a stress-crack opening constitutive law composed of a bilinear stress-crack opening relationship having two descending branches with decreasing negative slope [86].

The anchorage was modeled using an open-source finite element software, in which the author implemented Eqs. (1–6), and the above described tensile and cracking relationships.

The non-linear numerical model allows reliable and comprehensive results to be obtained, but the application of the model requires spending a lot of time and effort. All things considered, this non-linear numerical model is useful and applicable to the research, but definitely it is not easily usable and applicable to the profession.

The non-linear numerical model was therefore used to carry out a wide-ranging analysis, which included an exhaustive variety of geometries and materials of anchors and concretes. The results of that analysis allowed the behavior shared by concrete shear anchors to be identified. Afterwards, that behavior was expressed in the form of mechanical assumptions. Those assumptions allowed an analytical model to be constructed.

The results of the numerical analysis and the behavior shared by the shear anchors embedded into concrete is described in the following Subsections 5.1 and 5.2, while the assumptions established from those behaviors are stated in Section 6.

5.1. Results of the numerical analysis

Modeling encompassed the single anchor with both strong shaft and sufficient clearance from the edges. Therefore, failure was ever dictated by the concrete surrounding the anchor.

The displacements of the anchor induced by the shear force were found to be the result of substantial strains in the concrete, while the strains in the anchor and in the anchoring material were negligible. That results demonstrated hence that the anchor undergoes a rigid body motion (Fig. 3).

More specifically, the deviations from the rigid body motion resulted to be definitively negligible if the ratio between the length L and the diameter Ω of the anchor is: $L/\Omega \leq 24$ (slenderness ratio limit). For greater ratios, the bending behavior of the anchor is no more negligible. It is to note that the slenderness limit of [73] is 8. This numerical analysis has hence proven that the anchor can be slenderer than the limit prescribed by the ACI Committee.

In the case of the adhesive anchor with resin (which is soft compared to mortar), when the gap between the anchor and the drilled hole (i.e., the thickness of the anchoring material) respected the limits defined in [1], then the relative displacement of the anchor to the drilled hole was proven to be insignificant. When on the other hand, those limits were not respected, the relative displacement was proven to be significant.

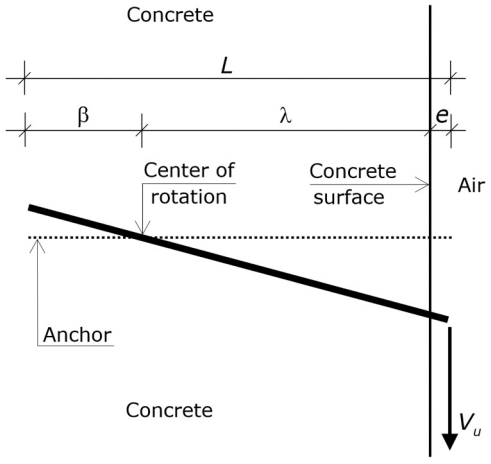

Fig. 3. Failure mode of an anchor post-installed into concrete, with $L/\Omega \leq 24$. The assumed failure mode ignores the extra-strength provided by the fixture, which makes the segment e bend (as that extra strength is no more than moderate).

Anchor's displacement can hence be decomposed into a translation and a rotation. The translation was discovered to be ever small and its contribution to be ever negligible with respect to the contribution of the rotation. Thus, the translation is hereinafter ignored.

Eventually (Fig. 3), the movement of the anchor was proven to consist of a rigid rotation around a center. The distance between the concrete surface and the rotation center is denoted by λ and the distance between the embedded end and the rotation center by β, with $\lambda > \beta$ and $L = \lambda + \beta + e$.

The drilled hole can be split into two cylinders, one of length λ and the other of length β, which in turn can be split into two half cylinders, one with positive y (lower half-cylinder of length λ, as the positive direction of y is that of V, and therefore the y-axis is directed downwards, as shown by Figs. 1 and 2), and the other with negative y (upper half-cylinder of length β). The rotation makes the anchor push against the surface of the half-cylinder of length λ oriented towards the positive y (lower one) and detach from the surface of the complementary half-cylinder of length λ (upper one), and vice versa for the half-cylinders of length β.

That pushing action generates contact pressures, which are exchanged between the concrete and the embedded system. Those pressures are parallel to the shear force (i.e., are directed along the y-axis), and are smeared both across the entire width (x-axis) and along the entire length (z-axis) of two above-mentioned half-cylinders that the anchor presses against. The contact pressures are denoted by p_c.

Ultimately, the contact pressures p_c acting on the concrete half-cylinder whose length is λ (lower half-cylinder) are directed along the positive y-direction (as V), while the contact pressures p_c acting on the concrete half-cylinder whose length is β (upper half-cylinder) are directed along the negative y-direction. The same contact pressures but with opposite direction (sign) act on the anchor (on the embedded system).

The contact pressures acting on the anchor equilibrate the shear force V applied at the external end of the anchor. On the other hand, the contact pressures having equal but opposite direction that act on the concrete dictate the shear strength of the anchor, since failure is governed by the concrete that surrounds the anchor, as proven by the numerical results and explained in the following.

The detachment of the anchor and anchoring material from the other half-cylinders was found to generate interface tensile stresses, which resulted either to be marginal or to crack the concrete and then to disappear. In the case of mechanical anchor, those tensile stresses resulted to be zero even in the uncracked concrete. Thus, the tensile stresses in the concrete are hereinafter ignored.

The numerical results showed that, if the external end is connected to a steel plate (with a nut or a weld) or is embedded into concrete or timber, then the shear strength of the anchor is greater than if it is free. Nevertheless, as previously anticipated and as found in [1] for the masonry shear anchor, that increase in strength was found to be significant only if the diameter of the anchor is particularly large, while for the anchors that are commonly employed that supplementary strength was found to be no more than moderate (more often small than not). As such, it is neglected. The external end is hence modeled as free. The role played by the plate in anchor's shear strength will be studied at the next research step.

From a certain level of the shear force onward, some concrete strains were found to exceed the pseudo-elastic limit. Increasing further the shear force, the rotation of the anchor increased progressively quicker, i.e., resulted in a decrease in the stiffness of the anchorage.

Eventually, at a certain anchor's rotation, the shear force at the external end could not be increased any longer, and for further increases

in rotation the shear force that could be applied started decreasing. That rotation identifies the ultimate limit state of the anchor, and that shear force defines the shear strength of the anchor.

The shear force carried by an anchor was found both to increase kind of slowly when the anchor rotation approached the ultimate limit state and to decrease reasonably slowly when the anchor rotation increased from the ultimate.

The numerical modeling demonstrated hence that an anchor can guarantee a pseudo-plastic behavior for rotations from appreciably lower to substantially greater than the ultimate rotation.

Everything else being equal, the shear strength of an anchor embedded into uncracked concrete and that of an anchor embedded into cracked concrete resulted to differ marginally. The numerical results demonstrated that the former surpasses the latter of less than 4.4%. That result agrees with [50], where those differences were found to be lower than 3.5%.

The stress state that exists in the concrete prior the installation of the anchor was proven that does not influence the shear strength of the anchorage.

Due to the rigid body behavior of the anchor (Fig. 3), the compressive strains at the drilled hole have a bi-triangular profile along the z-axis (Fig. 4). Since $\lambda > \beta$, the strain profile is asymmetric. The maximum absolute value of the strains occurs at the concrete surface.

At the ultimate limit state, the strain at the concrete surface resulted to differ no more than marginally from ε_{c1}, i.e., at ultimate the strain at $x = 0$; $y = \phi/2$; $z = 0$ (on the drilled hole at the outer concrete surface) was discovered to be almost equal to 2.2‰.

At ultimate, the strain at the embedded end, which is denoted by ε_β, was found to be ever pseudo-elastic, i.e., lower than the strain ε_L defined in Section 5.

The contact pressures p_c are the result of those compressive strains of the concrete at the drilled hole and of the non-linear constitutive law of concrete (Eqs. 1, 3, 4). Accordingly, two stress profiles act on the anchor – namely, one from $z = 0$ to $z = \lambda$ with negative direction and one from $z = \lambda$ to $z = L$ with positive direction. Of course, the same stresses act on the concrete with opposite directions.

The numerical results demonstrated that the resultant force of the stress profile acting onto the segment λ and its application point depend only on the maximum value of the contact pressure and λ, while they do not depend on the shape of the stress profile. That outcome was (and is) the result of the pseudo-plastic behavior of the anchorage.

That result allowed the stress profile from $z = 0$ to $z = \lambda$ at ultimate to be replaced by a resultant force and an application point that depend only on p_c and λ, which drastically simplified the analytical model that was constructed based on the numerical output.

The resultant force of the contact pressures acting on the segment λ of the drilled hole at ultimate of any anchor, which is denoted by F_λ, was

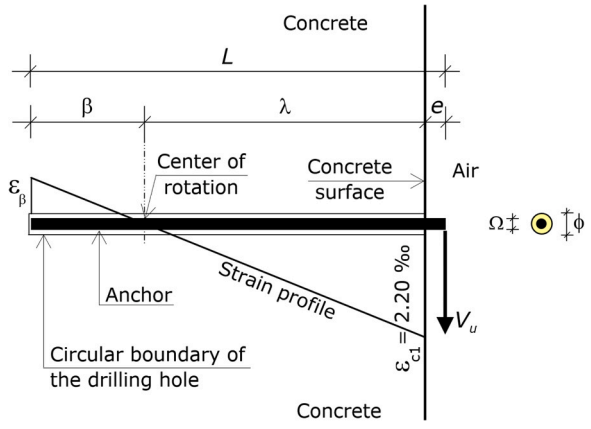

Fig. 4. Profile of the compressive strains at ultimate along the concrete that shapes the drilled hole.

proven to be well approximated by the following equation:

$$F_\lambda = 0.84 \cdot \left(\frac{p_{cm}}{33.0}\right)^{0.11} \cdot \phi \cdot \lambda \cdot p_{cm} \tag{7}$$

whose units are N and mm (the pressures are expressed in N/mm^2 while F_λ in N). Consequently, the model requires expressing each quantity in N and mm.

In Eq. (7), p_{cm} is the maximum contact pressure tolerated by the concrete. The resultant force F_λ acting on the anchor and the shear force V are parallel and oppositely directed.

Moreover, the distance between the application point of F_λ and the rotation center, which is denoted by d_λ, was proven to be well approximated by the following expression:

$$d_\lambda = 0.58 \cdot \lambda \tag{8}$$

Ultimately, Eqs. (7) and (8) exhibit only negligible differences from the values obtained from the non-linear numerical analysis and therefore they can be used in lieu of the actual stress profiles.

The stresses σ_z, τ_{zx}, and τ_{zy} resulted to be negligible. The principal stresses in the third direction, σ_3, resulted to be negligible too because it differs marginally from σ_z. The stress state was hence proven to be two-dimensional, which is in agreement with [1].

The fact that σ_3 and σ_z are negligible implies only that they can be taken as zero, not that they play no role. Indeed, $\sigma_3 = 0$ entails that the concrete is not confined in the z direction, while it is confined in the other two directions. That basic behavior drastically differentiates concrete anchor from masonry anchor because it implies a failure envelope different than that of masonry [1].

As proven in [1], the shear anchor generates a biaxial compressive stress state in the concrete. Let us consider the two-dimensional stress state in the x-y plane at a given z. The numerical results have proven that the major principal stress σ_1 and minor principal stress σ_2 can be accurately expressed by the following formulas:

$$\sigma_1(z) = \frac{p_c(z)}{\pi} \cdot [\alpha + sin(\alpha)] \tag{9}$$

$$\sigma_2(z) = \frac{p_c(z)}{\pi} \cdot [\alpha - sin(\alpha)] \tag{10}$$

where compressions are positive. Hence, those formulas define and quantify the above-described biaxial compressive stress state that the shear anchor induces in the concrete.

The bi-axial stress state described by Eqs. (9) and (10) holds true for cracked concrete too, as long as at least a narrow and short strip of concrete around the anchor and parallel to the shear force is uncracked before inserting the anchor. The reason is that the maximum compressive stress occurs near the anchor. The dimensions of that strip are in proportion to ϕ. However, a width of 150 mm and a length of 400 mm are adequate to almost any anchor.

5.2. Maximum compressive contact pressure

Eq. (7) requires knowing the maximum contact pressure p_{cm} that the concrete can resist. According to Eqs. (9) and (10), σ_1 and σ_2 at z depend only on p_c at z (while $\sigma_3 = 0$). So, the principal stresses do not depend on the profile of the contact pressures along z, but only on the contact pressure p_c at z.

On one hand, the compressive principal stress σ_1 is greater than the compressive principal stress σ_2, as the former is the maximum principal stress (in absolute value). On the other hand, however, the latter was found to be not appreciably lower than the former around the drilled hole.

The two principal stresses σ_1 and σ_2 play two opposite roles in the ultimate behavior of the concrete. The maximum compressive principal stress $\sigma_1(z)$ is the contact pressure that resists the shear force, while the

compressive principal stress $\sigma_2(z)$ confines the concrete in the y-direction. However, the minimum principal stress σ_3, which is nil, provides the concrete with no confinement in the z-direction. As a result, the total confinement action is not great, although not negligible.

Eq. (9) shows that the maximum σ_1 occurs at $\alpha = \pi$. Eq. (10) shows that the maximum σ_2 occurs at $\alpha = \pi$. The two maxima occur hence at the same point, whose Cartesian coordinates are $x = 0$, $y = \phi/2$, $z = 0$.

Since the confinement provided by σ_2 is no more than moderate (given that σ_3 is zero), the maximum compressive contact pressure p_{cm} depends much more on σ_1 than on σ_2. The stress state that dictates p_{cm} is thus dictated by the principal stresses at $\alpha = \pi$ and its principal stresses are $\sigma_1 = p_{cm}$ (compression), $\sigma_2 = p_{cm}$ (compression), and $\sigma_3 = 0$.

All the acceptable formulations show that the increase in strength due to a biaxial confinement is much lower than that provided by a triaxial confinement, as well substantially lower than that due to biaxial confinement of masonry [1]. The Mohr-Coulomb failure criterion that can be used for masonry is hence here not valid, as it describes the conditions for which an isotropic material will fail, with any effect from the principal stress σ_3 being neglected.

The compressive strength f_{cm} of the above-described stress state can be taken as:

$$f_{cm} = 1{\cdot}15{\cdot}f_c \tag{11}$$

where f_c is the strength of concrete under a uniaxial state of stress.

Eq. (11) was derived from the models of literature that best agree with test data about bi-axial stress state of concrete, so that (11) is at the same time an accurate and safe estimation. It is to note that f_{cm} from (11) was used in Eqs. (1), (2), and (4) too.

Combining Eq. (11) and the stress state at the point $\alpha = \pi$, the maximum contact pressure p_{cm} turns out to be:

$$p_{cm} = 1{\cdot}15{\cdot}f_c \tag{12}$$

Ultimately, p_{cm} to use in Eq. (7) is that provided by Eq. (12).

6. Mechanical assumptions

The ultimate behavior depicted in Subsections 5.1 and 5.2 can be captured by five mechanical assumptions.

1. Stresses in the concrete are induced only by the compressive contact pressures due to the shear force V_u.

2. The compressive strain along the drilled hole (along z) is an asymmetric bi-triangular profile that at $x = 0$; $y = \phi/2$; $z = 0$ is equal to 2.2‰, at $z = \lambda$ is zero, and at $z = \lambda + \beta$ is equal to the strain ε_β which is lower than the pseudo-elastic limit ε_L.

3. For a given z, the compressive strain is uniform for y from $-\phi/2$ to $+\phi/2$.

4. The resultant force F_λ of the compressive contact pressures acting on the segment λ at ultimate is defined by Eq. (7), in which p_{cm} is given by Eq. (12).

5. The distance d_λ of the point of application of F_λ from the center of rotation is defined by Eq. (8).

By virtue of Assumption 1, the only stresses to consider are those induced by the anchorage. Neither the position at which the anchor is installed, nor the direction of the shear force has thus any influence. By virtue of Assumption 1, moreover, the tensile interface stresses can be neglected.

Assumption 2 and 3 imply that the ultimate profile of the compressive strains along the concrete that shapes the drilled hole (i.e., along z) is a plane strip of width ϕ, which starts from a known value and passes through the rotation center (uniform strains along any semi-circumference of the drilled hole, i.e., along y).

Assumption 2 also implies neglecting the strengthening effect provided by the plate (fixture). By virtue of Assumption 2, the resultant force F_β of the contact pressures acting on β at ultimate is produced by elastic contact pressures. Assumption 2 and 3 imply that the profile of the strain at the interface between concrete and embedded system is straight, which allows ε_β to be defined. Actually, Assumption 3 is not strictly necessary. It has been made only for the sake of clarity.

Assumption 4 provides the magnitude of the resultant force F_λ produced by the contact pressures acting on the segment λ at ultimate, while Assumption 5 provides the position of F_λ at ultimate.

7. Analytical model

The five assumptions allow the analytical model to be constructed. The strain at the anchor's internal end ε_β can be derived from Assumption 2 and 3 (Fig. 4):

$$\varepsilon_\beta = 0.0022{\cdot}\frac{\beta}{\lambda} \tag{13}$$

The stress σ_β produced by ε_β can be obtained using the elasticity modulus of the concrete E_c:

$$\sigma_\beta = 0.0022{\cdot}\frac{\beta}{\lambda}{\cdot}E_c \tag{14}$$

The resultant force of the contact pressures acting on β at ultimate, which has been denoted by F_β, is equal to the volume of a triangular prism whose sides are β, ϕ, and σ_β:

$$F_\beta = \frac{\phi{\cdot}\beta{\cdot}\sigma_\beta}{2} \tag{15}$$

The force F_β is transverse to the anchor and parallel to V_u, with the same direction (Fig. 1). Replacing σ_β with Eq. (14), Eq. (15) becomes:

$$F_\beta = 0.0011{\cdot}\phi{\cdot}\frac{\beta^2}{\lambda}{\cdot}E_c \tag{16}$$

Given that the resultant force F_β is applied at the centroid of that prism, the distance of F_β from the rotation center, which is denoted by d_β, is equal to:

$$d_\beta = \frac{2{\cdot}\beta}{3} \tag{17}$$

The remaining unknowns of the problem are 1- the position of the rotation center; 2- and the ultimate shear force V_u, which is what the model aims at predicting.

The rotational equilibrium equation around the anchor's end protruding from the concrete gives:

$$F_\beta{\cdot}\left(d_\beta + \lambda + e\right) - F_\lambda{\cdot}(\lambda - d_\lambda + e) = 0 \tag{18}$$

Using Assumption 4 and 5, and plugging Eqs. (15) and (17) into Eq. (18), the following equation turns out:

$$0.0011{\cdot}\phi{\cdot}\frac{\beta^2}{\lambda}{\cdot}E_c{\cdot}\left(\frac{2{\cdot}\beta}{3} + \lambda + e\right) - 0.84{\cdot}\left(\frac{p_{cm}}{33.0}\right)^{0.11}{\cdot}\phi{\cdot}\lambda{\cdot}p_{cm}{\cdot}(0.42{\cdot}\lambda + e) = 0 \tag{19}$$

where p_{cm} is given by Eq. (12).

The diameter ϕ can be eliminated from (19), as it is obviously different than zero.

$$0.0011{\cdot}\frac{\beta^2}{\lambda}{\cdot}E_c{\cdot}\left(\frac{2{\cdot}\beta}{3} + \lambda + e\right) - 0.84{\cdot}\left(\frac{p_{cm}}{33.0}\right)^{0.11}{\cdot}\lambda{\cdot}p_{cm}{\cdot}(0.42{\cdot}\lambda + e) = 0 \tag{20}$$

Eq. (20) shows that the position of the rotation center depends neither on the diameter of the anchor Ω nor on the diameter of the drilled hole ϕ, but only on the strength and stiffness of the concrete.

Both β and λ are unknown, which would make it seem that Eq. (20)

has two unknowns. Nevertheless, the geometric relationship shown by Fig. 1 relates β and λ, i.e., $\beta + \lambda + e = L$. That relationship allows β to be expressed as a function of λ, or vice versa. In so doing, Eq. (20) is transformed into an equation with only one unknown, whose solution provides λ (or β). Then, the relationship between λ and β gives β (or λ).

The problem can then be solved using the condition for the translational equilibrium of a rigid body in the direction of V:

$$F_\beta - F_\lambda + V_u = 0 \rightarrow$$
$$V_u = 0.84 \cdot \left(\frac{p_{cm}}{33.0}\right)^{0.11} \cdot \lambda \cdot \phi \cdot p_{cm} - 0.0011 \cdot \phi \cdot \frac{\beta^2}{\lambda} \cdot E_c \quad (21)$$

All the quantities on the right of Eq. (21) are known, which allows V_u to be obtained.

In brief, the analytical model consists of Eqs. (20) and (21). The data of the model are the length L and the diameter ϕ of the drilled hole, the eccentricity e of the external end, and the uniaxial crushing (compressive) strength of the concrete f_c, while the maximum contact pressure tolerated by the concrete p_{cm} and the elasticity modulus of the concrete E_c can be obtained from f_c using Eqs. (12) and (2), respectively, with f_{cm} of Eq. (2) given by Eq. (11).

Eqs. (20) and (21) are expressed in closed form. Once β is replaced by a function of λ (or vice versa) in (20), the two-equation system has two unknowns. Once λ (or β) is obtained from (20), and then β (or λ) is obtained from the above geometric relationship, those values, together with p_{cm} and E_c, shall be plugged into (21). In so doing, V_u is eventually obtained.

The explicit solution is not presented since the formulas would be, not only cumbersome, but above all useless. In fact, it is much easier to solve the two-equation system using a computer program (e.g., *Matlab*). Nevertheless, Section 10 presents a simplified expression.

8. Experimental verification of the analytical model

The author used professional cases of which he was both the structural designer and the works supervisor as an opportunity to perform experiments devoted to verifying the predictive capacity and accuracy of the analytical model.

The author first designed the experiments, then directed the on-site testing, and finally analyzed the collected experimental results. The experimental activity consisted of 16 failure tests.

8.1. Specimens that were tested to failure

The anchors were made of steel and were post-installed into concrete walls. The 16 tests – data and results – are reported in Table 1.

Every concrete portion where an anchor was post-installed, had been previously tested in order to know its compressive strength. To that end, samples of concrete were extracted from the walls (using a core drill) and were brought to a laboratory, where they were loaded axially until failure, so as to measure the concrete compressive strength. The concrete was also tested on site using the rebound hammer (Schmidt hammer) and measuring the ultrasonic pulse velocity, according to the *Sonreb* method. Every slenderness ratio of the anchors that were tested satisfied $L/\Omega \leq 18$.

8.2. Test method and test set-up

The author designed a test set-up, which is applicable and useful for shear testing any anchor (Figs. 5 and 6). In fact, the Author had used this test set-up for testing the masonry anchors of [1] and will use it to carry out the other steps of this research.

The test set-up is comprised of a hydraulic jack, the control unit, two adhesive steel anchors, a steel beam of I-section, a steel bar of square section (alongside a steel plate, as an alternative to the steel bar), and two displacement transducers.

The testing method is comprised of the following steps. The anchor to be tested and two adhesive anchors are post-installed into the concrete, the former above and the latter below at the same height. The steel beam is then placed onto those two anchors and the jack is placed between that beam and the anchor to be tested. The jack is supported by the former one and is connected to the latter ones by means of a steel bar having tiny square section, which concentrates the force of the jack onto a small area of the anchor's length. Every component of the test set-up is substantially stronger and stiffer than the anchor to be tested.

The experiments have proven that neither the direction of the force nor the stress state due to the loads of the building affects the shear strength of the anchor. If the jack is underneath the tested anchor, the potential for harm in terms of human injury or ill-health, and damage to structure is minor, while if it is above the hazard is substantially greater. With all of this considered, the test set-up applies the force to the tested anchor from below, while in reality the attachment applies the force to the anchor from above.

8.3. Shear tests

The tests were performed using the set-up described in Subsection 8.2 (Figs. 5 and 6). In each test, the force applied by the jack to the anchor was increased from zero up to the complete collapse of the anchorage (Figs. 7–11 and 13).

Figs. 7–11 show some of the shear tests that were performed. Fig. 12 shows two force-displacement curves. Fig. 13 shows the failure mode, i.e., concrete crushing. The walls where the anchors were embedded were coated by plaster. In all the tests, the plaster was not removed because it allowed concrete crushing to be better observed without altering the behavior of the anchor (the plaster was neither thick nor hard). Each load process included some unloadings, in order to identify the pseudo-elastic limit of the anchorage (Fig. 12).

Each test measured the ultimate shear force resisted by the anchor, i.e., the maximum shear force carried by the anchorage (Table 1), and the load-displacement curve, i.e., the response of the anchorage to the shear loading (Fig. 12).

Table 1
Shear strengths measured by the tests and predicted by the model, for 16 anchors embedded into concrete. 1st row: number of the case study (S1-S16). 2nd, 3rd, 4th, 5th rows: mechanical and geometric parameters of each anchor, which allow Eqs. (20) and (21) to be applied. 2nd to last row: anchor's shear strength $V_{u\text{-}exp}$ measured by the test (with one digit after the decimal point). Last row: anchor's shear strength V_u predicted by the analytical model (with two digits after the decimal point). 1st and 2nd columns: symbols and relevant units. Columns from the 3rd to the last: number of each of the 16 tests, data, experimental result, i.e., $V_{u\text{-}exp}$, and theoretical prediction of the model, i.e., V_u.

		S1	S2	S3	S4	S5	S6	S7	S8	S9	S10	S11	S12	S13	S14	S15	S16
f_c	N/mm^2	9.0	10.0	12.0	14.0	16.0	18.0	20.0	20.0	23.0	26.0	28.0	30.0	35.0	40.0	42.0	45.0
L	mm	126.0	138.0	160.0	172.0	192.0	212.0	227.0	255.0	224.0	241.0	246.0	290.0	318.0	278.0	370.0	397.0
ϕ	mm	10.0	12.0	12.0	12.0	14.0	16.0	18.0	20.0	20.0	22.0	24.0	26.0	28.0	30.0	35.0	40.0
e	mm	6.0	8.0	10.0	10.0	12.0	12.0	7.0	5.0	14.0	11.0	16.0	15.0	18.0	18.0	20.0	22.0
$V_{u\text{-}exp}$	kN	4.7	6.7	9.0	11.7	16.8	23.2	33.7	42.4	38.3	52.2	59.0	84.4	123.9	131.6	226.7	302.1
V_u	kN	4.27	6.11	8.48	10.82	16.01	23.15	33.08	42.41	38.80	54.29	62.17	88.08	120.27	126.41	211.91	277.73

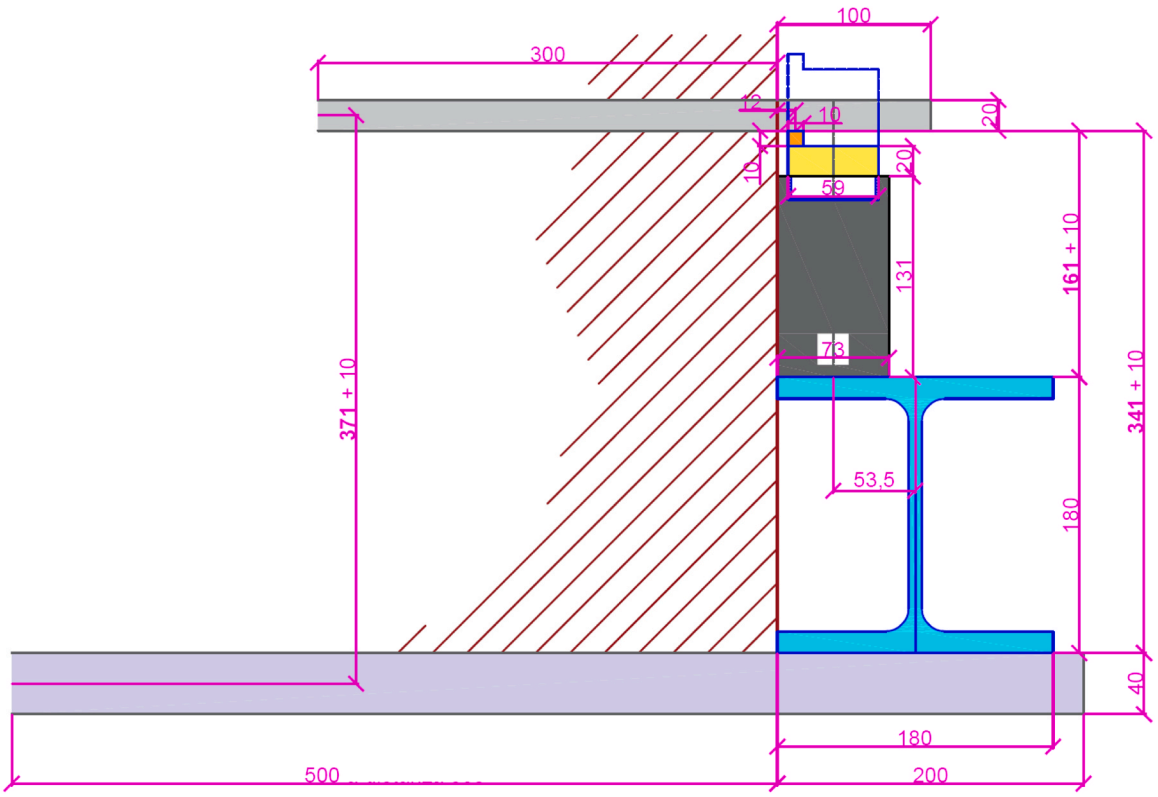

Fig. 5. Test set-up represented for the anchor with $\Omega = 20$ mm and $L - e = 300$ mm: cross section of the concrete wall and longitudinal section of the tested anchor embedded into the wall (the anchor above in the drawing). The figure shows the jack (a cylinder with a head). The jack applies the shear force to the bottom of the anchor through a steel bar of square section, which reduces the eccentricity of the shear force. The figure also shows the I-section steel beam that collects the reaction force of the jack, which is supported by two anchors of large diameter and long embedded length.

8.4. Analysis of the experimental results

The shear force applied by the test set-up to the tested anchors was directed upwards, while the shear force applied by an attachment to an anchor is directed downwards. According to Assumption 1, however, the direction of the vertical shear force has no influence on the behavior of the anchor. For the sake of avoiding confusion, the analysis of the experimental results takes the positive direction of the y-axis as upwards (in the Cartesian coordinate system shown in Fig. 2 the y-axis is hence upwards), i.e., the positive direction is taken to be that of the shear force applied in the experiments.

The nominal steel strength of the tested anchors (carbon steel) was 650 N/mm^2, while the nominal yield strength was 520 N/mm^2.

Failure of every tested anchorage was dictated by the concrete that surrounded the anchor (Fig. 13), i.e., the failure mode was always that reproduced by the model (shown in Fig. 3).

The shear strengths measured by the tests are reported in Table 1 (symbol $V_{u\text{-}exp}$) together with the relevant parameters. Each load value given in Table 1 is the peak of the relevant load-displacement curve.

Fig. 12 reports the load-displacement curves of two tests. The ordinate shows the loads, i.e., the shear force applied by the jack at each loading step. The abscissa shows the displacements, i.e., the vertical translation at each loading step of the point of the masonry surface at $x = 0$, $y = \phi/2$, $z = 0$. Those two curves are representative of all the experiments performed.

The behavior of the tested anchors met closely with the assumptions of the analytical model, which was expected as the assumptions had been derived from a sophisticated non-linear numerical modeling. For instance, the validity of Assumption 2 was confirmed by the fact that the embedded part of each anchor underwent no more than elastic deformations (Fig. 10).

The two curves of Fig. 12, as well as the other 14 load-displacement curves, exhibit a significant elastic behavior, followed by an elasto-plastic and then a plastic behavior, which are as much significant. The 16 curves also show that the ultimate displacement and plastic deformation (rotation) of each tested anchor are large, so that the shear strength is dictated by the maximum contact pressure carried by the concrete p_{cm} and not by the rupture strain of the concrete.

8.5. Comparison between the theoretical predictions and the experimental results

Each test was simulated with the analytical model. Each theoretical prediction is reported in Table 1, together with the shear strength from the experiment, which allows the former to be compared to the latter.

The comparison shows that for every anchor, the difference between the predicted shear strength and the experimental shear strength was within $\pm$ 10%. Not only is that range of deviations small, but also it corresponds to the accuracy of the tests performed for estimating the concrete compressive strength of each structure (in-place tests and laboratory tests by drilling and testing core samples).

Ergo, the test results verified the capacity of the analytical model presented in Section 7 to accurately predict the shear strength of an anchor embedded into concrete.

9. Experimental results attainable from the literature

The accuracy of the model was also tested borrowing experimental results from the scientific literature. The anchors experimented in [9, 32, 50] failed by the rupture of the surrounding concrete. Those tests can therefore be simulated by this model. Those experimentations included the measure of the strength of the concrete and steel.

The free parameters to insert into the model for the 12 anchors tested in [9] are: $L = 169$ mm or 219 mm; $\phi = 19$ mm (3/4″); $e = 10.0$ mm; f_c

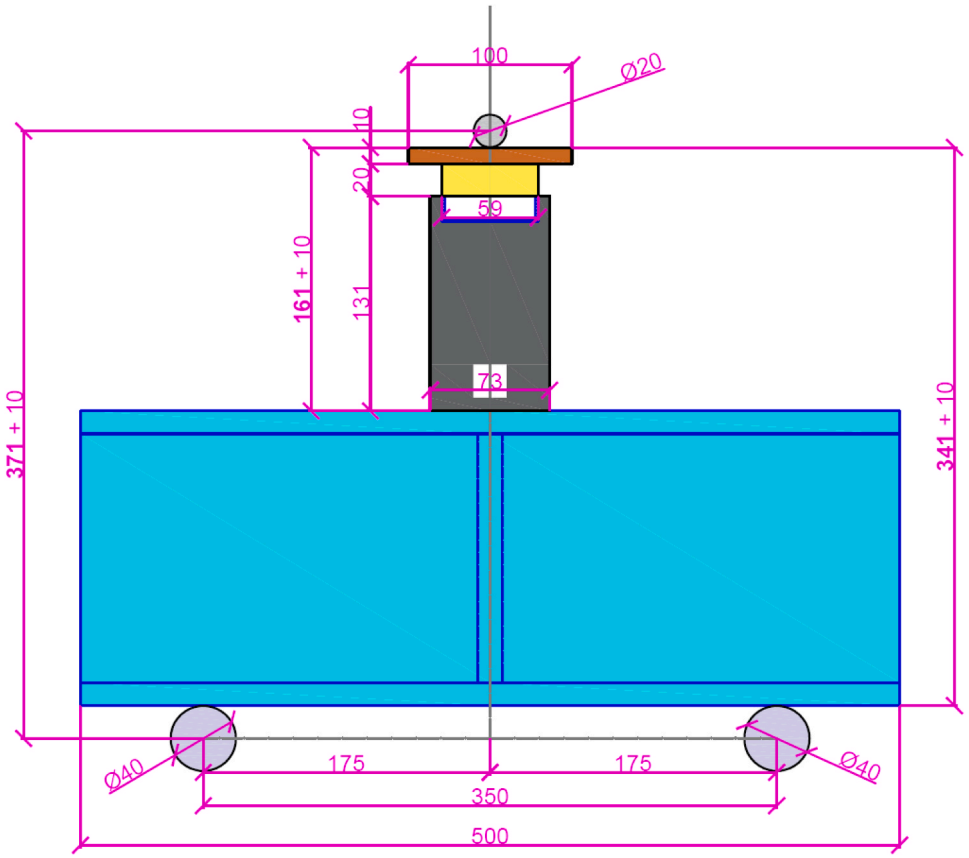

Fig. 6. Test set-up represented for the anchor with $\Omega = 20$ mm and $L - e = 300$ mm: frontal view (the cross section cuts the set-up but not the concrete). The jack (a cylinder with the head that moves along the vertical axis) pushes the steel bar (transverse to the tested anchor), which in its turn pushes the anchor's segment protruding from the concrete surface (the anchor above in the diagram). The I-section steel beam that supports the jack is simply supported by the two lower anchors and is stiffened by a transverse plate welded at its midspan. The test set-up applies the shear force from downwards (as this is the safest test arrangement).

$= 46.1$ N/mm^2. For $L = 169$ mm, the model gives $V_u = 51.11$ kN, and for $L = 219$ mm gives $V_u = 76.13$ kN. The average shear strength measured in the 6 tests with $L = 169$ mm was $V_u = 64.38$ kN, and in the 6 tests with $L = 219$ mm was $V_u = 90.5$ kN. The experimental results are hence 20.6% and 15.9% more, respectively, than the theoretical predictions, which is a satisfactory result because each tested anchor had a heavy hex nut at the embedded end.

The free parameters to insert into the model for the 2 anchors tested in [50] are: $f_c = 38.5$ N/mm^2; $L = 112$ mm; $\phi = 10.0$ and 12.0 mm; $e = 12.0$ mm. For $\phi = 10.0$ the model gives $V_u = 14.66$ kN and for $\phi = 12.0$ mm gives 19.91 kN. The shear strengths measured by the tests were $V_u = 15.85$ kN and 24.52 kN for the 10-mm and 12-mm anchors, respectively. The experimental results are hence 7.5% and 18.8% more than the theoretical predictions, which is a satisfactory result because the test set-up provided the anchors with extra strength.

The free parameters to insert into the model for the anchor tested in [32] are: $f_c = 60.1$ N/mm^2; $L = 405$ mm; $\phi = 20.0$ mm; $e = 12.5$ mm. For those values, the model gives $V_u = 201.1$ kN. The shear strength measured by the test was $V_u = 231.0$ kN, which is 14.9% more than the theoretical value. That result is satisfactory because the tested anchor had a nut at the embedded end.

10. Simplified analytical expression

In order to allow the structural designer to take the initial choices when the anchor is one of the options, this research effort has tested whether or not the simplified formula proposed in [1] for the masonry anchor, i.e., Eq. 20 of that paper, can be used for the concrete anchor, at least for making a first and rough approximation only.

That formula was found to be capable of providing predictions that, although not conservative, are not drastically far from those given by the analytical model, i.e., Eqs. (20) and (21). Thus, that formula can be borrowed from [1] and applied to the concrete anchor. The shear strength from that formula is denoted by $V_{u\text{-}max}$:

$$V_{u\text{-}max} = 0{\cdot}414{\cdot}\phi{\cdot}L{\cdot}q_{mc} \tag{22}$$

where q_{mc} is the maximum contact pressure that the anchor can transmit to the concrete.

Eq. (11) allows q_{mc} to be replaced by f_c:

$$V_{u\text{-}max} = 0{\cdot}476{\cdot}\phi{\cdot}L{\cdot}f_c \tag{23}$$

Ultimately, Eq. (23) is a simplified formula devoted to assisting the structural designer when he has to decide whether the shear anchor is a viable solution in order to connect an attachment to a concrete structure. On the contrary, that formula should be used neither to execute safety verifications nor to design the anchor.

11. Discussion

The marginal differences between the theoretical predictions and the experimental results are the logical outcome of the way the analytical model has been constructed, as it is based on the results of a wide-ranging analysis performed with a sophisticated non-linear numerical model.

It is hardly necessary to mention that the analytical model was not calibrated against the results of those experiments, as it is a predictive model. Accordingly, this model is devoted to describing the behavior of any anchor, and not only of the anchors that were tested, as it occurs for

Fig. 7. Shear test performed using the procedure presented in Section 8. This test used a steel plate in lieu of the square-section steel bar because in so doing the eccentricity was lower (that bar appears on the I-section, unused).

Fig. 8. Shear test performed on an anchor embedded into a concrete wall. The plaster was not removed before the test because on one hand, it did not alter the behavior of the anchor, while on the other hand, it allowed concrete crushing to be better observed and identified.

empirical formulations.

As expected, by enlarging the embedded depth $L - e$ the load-bearing capacity of the shear anchor extends and heightens, but only as long as the slenderness ratio L/Ω is lower than the rigid body limit. The slenderness ratio limit for which the anchor exhibits a rigid body behavior resulting from this research is considerably higher than that suggested in [73], i.e., 24 in lieu of 8.

A less expected result is that all the rest being equal, the greater the diameter of the drilled hole ϕ the greater V_u, while the diameter of the anchor Ω has no influence on V_u. In short, anchor's shear strength depends on ϕ but not on Ω.

That result implies that, everything else being equal, the gap between anchor and drilled hole of adhesive anchor makes it stronger compared to mechanical anchor (in the former $\phi > \Omega$, while in the latter $\phi = \Omega$). Furthermore, the gap of the anchor bonded with mortar anchoring material makes it stronger compared the anchor bonded with resin anchoring material ($\phi - \Omega$ of the former is greater than that of the latter). However, the choice of which anchor to use depends on the project at hand.

The analytical model presented in this paper was applied to a wide range of anchorages representative of the variety of real cases. The results of that application have shown that, if the anchor is well designed, properly installed, and optimally placed, it definitely fails by the mode shown in Fig. 3, as the shear strength predicted by the analytical model is ever lower than the shear strength of every other failure mode. Therefore, as long as there is sufficient clearance from both the edges and other anchors, and the shaft is sufficiently strong, anchor's shear strength is dictated by the failure of the concrete in front of the anchor, and hence its value is that predicted by this model.

It is hence expected that the relevant codes will be reviewed, in order to incorporate this failure mode (e.g., [73,74,83], which ignore the shear strength of the anchor dictated by the failure of the concrete in front of the anchor).

What seems to be an exception is the case of the anchor with a particularly large diameter, made of a strong steel, and post-installed into a concrete with a relatively flat downward slope of the σ-ε softening curve. That anchor can bear a shear force greater than the shear force that has triggered the crushing of the concrete in front of the anchor. This extra-strength with respect to that predicted by this model is provided by the dowel action. The dowel mechanism depends however on the depth of the concrete along which the contract pressures decrease no more than slightly from the maximum contact pressure tolerated by the concrete p_{cm}, and this depth in turn depends on the actual downward slope of the concrete softening curve. The softening behavior of the concrete in front of the anchor is however difficult to predict. Therefore, that extra-strength should not be accounted for in safety assessment calculations, while it should be incorporated into the qualitative evaluations about the post-failure behavior of the anchor under design.

As reviewed in Section 3, the literature about anchors includes important experimentations, which are a landmark for theoretical activity. Some of them are [41,53,54,68], which present the above-mentioned specific phenomenon. That is, some tested anchorages allowed the applied shear load to be increased even after the concrete in front of the anchor had crushed and, owing to the dowel action, this increase continued up to the steel rupture. Nevertheless, those test results also showed that this phenomenon cannot be reliably predicted, as it depends on uncontrollable factors.

Fig. 9. Photo taken immediately after the test was completed. The image shows the anchor just tested, which is bent upward. This test used the square-section steel bar.

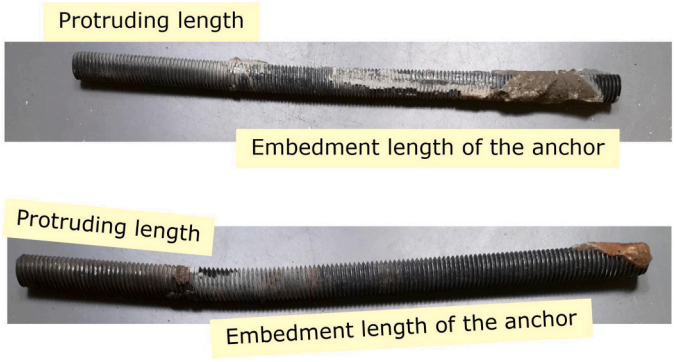

Fig. 10. Two anchors of different diameters and lengths extracted from the concrete after their test. All the anchors extracted from the concrete after the tests did not exhibit any plasticity in the embedded part, while the sections that emerged from the concrete surface sometimes exhibited large bending (e.g., the lower anchor in the figure).

The case studies of Table 1 were also analyzed using the provisions of two widely used documents edited by the American Concrete Institute, i.e., [73] and [74], which have been reviewed in Section 3. That state-of-the-art application has borrowed the formulations provided by Appendix B (Subsection B.6) of [73] and by Chapter 17 (Subsection 17.7) of [74]. More specifically, that application has used the formula B-15 taken from [73], with $f_{ut} = 1.75 \cdot f_y$, and the formulas 1a/b, 1.3, 2.1a/b, 2.2, 3.1, 4.1a/b, and 6.1 of Subsections 17.7.2, together with the

Fig. 11. This test used a set-up different than that described in Section 8. In this test, the force was applied by a jack that pulled the anchor and was restrained to a crane by means of a steel cable. This test was performed in the same building where a masonry shear anchor was tested as well [1], whose walls on the first story were made of concrete while on the upper stories were made of masonry.

formulas 1a/b of Subsections 17.7.3, taken from [74]. The formulas were applied using a distance of the anchor from the edge of 200 mm (7.847 in, as [73] uses imperial units), a depth of concrete of 800 mm (31.388 in) and high strength steel. In so doing, the effects of proximity to the edges, small depth of the concrete structure, and failure of the steel did not dictate the shear strength of the analyzed anchors.

Table 2 compares the shear strengths calculated using [73] and [74] to those obtained from this model. While the provisions from [73] and [74] are almost equal to each other, they are significantly different than the predictions of the analytical model. As shown in Table 2, not only do the formulations of [73] and [74] not provide accurate predictions, but also imply systematic errors, which derive from what has been pointed out in Section 3 and that can result in either an underestimation or an overestimation.

12. Conclusions

This research has tackled the problem of describing the ultimate behavior of the shear anchor post-installed into a concrete structure. This paper accounts for that activity and delivers a closed-form equation model that predicts the shear strength of an anchor embedded into concrete. That model can also be applied to an anchor group on condition that anchor spacing is not close.

The model requires knowing the uniaxial compressive strength of the concrete, the diameter and length of the anchor, and the length that protrudes from the concrete surface (i.e., 4 values).

The analytical model was constructed based on the results obtained from a refined non-linear numerical model. The complexity of the latter was concentrated in mechanical assumptions, based on which the former was derived. In so doing, the analytical model that was obtained is easy and fast to use, and at the same time it is just as accurate as the assumptions, which in their turn are as accurate as the non-linear numerical model.

Research activity included designing and carrying out 16 failure tests of 16 different steel anchors embedded in different concrete structures. The comparison between the theoretical results from the model and the experimental results from those tests has confirmed the reliability and accuracy of the analytical model.

Activity also considered experiments that are present in literature, which were reproduced by the analytical model. Once again, the comparisons were satisfactory.

The model applies to well designed, properly installed, and optimally placed anchors. Accordingly, failure is dictated by the concrete that

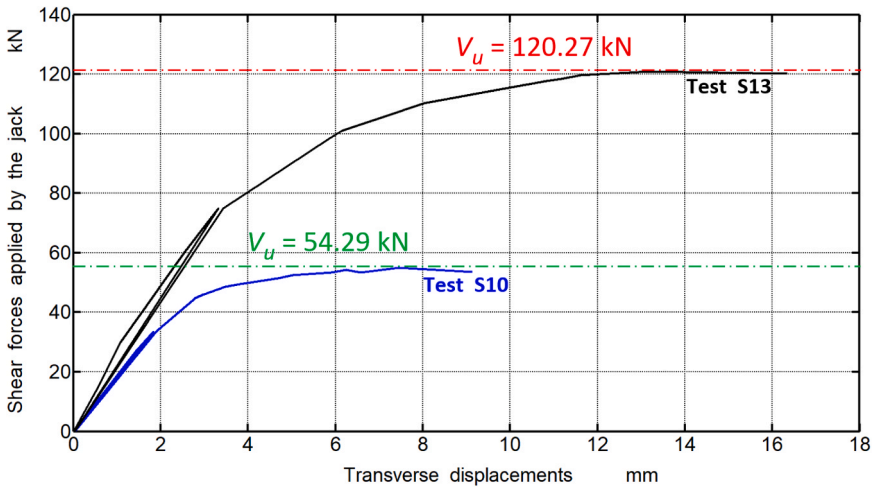

Fig. 12. Load-displacement curves of the 10th and 13th experiments of Table 1 (S10 and S13, respectively). Abscissa: vertical displacements of the anchor's cross-section at the concrete surface. Ordinate: transverse forces applied by the jack to the anchor. The descending branch of the curves was not represented, as it strongly depended on the way the jack was extended. The figure also shows the shear strength V_u of each tested anchor. For the sake of clarity, the diagram shows only the unloading from the elastic limit.

Fig. 13. Closeup of some anchors after the test showing the concrete crushing.

Table 2
Comparisons between theoretical predictions and code provision predictions. 1st row: number of the case study (S1-S16), which are those of Table 1. 2nd row: V_u from the analytical model, i.e., shear strengths reported in Table 1. 3rd row: shear strength from [73], which is denoted by $V_{u\text{-}a}$. 4th row: shear strength from [74], which is denoted by $V_{u\text{-}b}$. Each column compares thus the analytical result to ACI code provisions for each case study of Table 1.

		S1	S2	S3	S4	S5	S6	S7	S8	S9	S10	S11	S12	S13	S14	S15	S16
V_u	kN	4.27	6.11	8.48	10.82	16.01	23.15	33.08	42.41	38.80	54.29	62.17	88.08	120.27	126.41	211.91	277.73
$V_{u\text{-}a}$	kN	2.01	3.83	5.06	8.34	12.27	21.19	36.12	46.74	58.53	87.71	116.88	175.55	252.01	277.32	514.84	710.99
$V_{u\text{-}b}$	kN	2.11	3.91	5.88	8.28	11.97	20.95	36.81	47.02	66.61	96.03	129.11	214.12	290.27	300.91	499.21	694.13

surrounds the anchor, and not by the structural boundaries, the anchor group effect, or the metal shaft. Satisfaction of the above requirements shall be checked at the end of the analysis, by verifying that the shear strengths governed by the other failure modes are greater than the strength provided by this model.

Combinations of shear force and substantial tensile force are not included in this model. This is however not so much a behavior that is not covered by this model, but more about a connection between the attachment and the concrete that has not been designed in the best way.

Modern structural engineering has drastically reduced the use of analytical models and prefers using the finite element method implemented in the professional software codes. Nevertheless, there are structural problems that cannot be solved using the professional software codes that are currently available.

This paper has proven that the numerical analysis of a concrete anchor needs a three-dimensional model, together with non-linear constitutive laws of the materials and interfaces. The commercial software codes are not adequate to perform such analyses, while the software codes that can perform such analyses are not adequate outside university circles and outside research activity. The model that has been proposed in this paper makes a bridge between sophisticated non-linear numerical modeling and design activity of practitioners.

A remark made in Section 3 can also be suitable as a closing remark. Although the post-installed anchor behaves differently than the cast-in anchor, the post-installed anchor with adequate clearances from the boundaries (edges) and from other anchors (adequately spaced) has only been marginally dealt with by past published research, and even less by codes. In particular, not only does previous literature not provide researchers and practitioners with any analytical model, but above all ignores the failure mode due to concrete crushing, which leads to erroneous and potentially unsafe predictions. Therefore, there was a gap in literature regarding this issue. The author is confident that this paper has filled such a gap, and hopes that this model may be useful to academia research, as well as applicable to the professional and industrial activity.

CRediT authorship contribution statement

Foraboschi Paolo: Conceptualization, Data curation, Formal analysis, Funding acquisition, Investigation, Methodology, Project administration, Resources, Software, Supervision, Validation, Visualization, Writing – original draft, Writing – review & editing.

Declaration of Competing Interest

The author declares that he has no known competing financial interests or personal relationships that could have appeared to influence the work reported in this paper.

Data Availability

No data was used for the research described in the article.

References

[1] Foraboschi Paolo. Shear strength of the anchor embedded into masonry. Eng Struct 2023;294:116749 (n).
[2] Foraboschi Paolo. Ultimate shear force of an any anchor group post-installed into concrete. Materials 2023;16(7):2608 (n).
[3] Bogdanić Anton, Casucci Daniele, Ožbolt Joško. Numerical and experimental investigation of anchor channels subjected to shear load in composite slabs with profiled steel decking. Eng Struct 2021;240:112347.
[4] Brown Russell H, Whitlock ARhett. Strength of anchor bolts in grouted concrete masonry. J Struct Eng 1983;109(6):1362–74 (June).
[5] Cook Ronald A, Klingner Richard E. Ductile multiple-anchor steel-to-concrete connections. J Struct Eng – ASCE 1992;118(6):1645–65 (June).
[6] Divya M, Kumar RSenthil, George Prince, Jayabalan P, Tsavdaridis Konstantinos Daniel, Bahurudeen A. Development of novel shear connectors for cold-formed steel concrete composite beams. Constr Build Mater 2023;387:131644.
[7] Karmokar Trijon, Mohyeddin Alireza, Lee Jessey, Paraskeva Themelina. Concrete cone failure of single cast-in anchors under tensile loading – a literature review. Eng Struct 2021;243:112615.
[8] Lee Jong-Han, Cho Baiksoon, Kim Jae-Bong, Lee Kun-Joon, Jung Chi-Young. Shear capacity of cast-in headed anchors in steel fiber-reinforced concrete. Eng Struct 2018;171:421–32.
[9] Petersen Derek, Lin Zhibin, Zhao Jian. Experiments of cast-in anchors under simulated seismic loads. Eng Struct 2021;248:113197.
[10] Su Yusheng. Evaluation of the load-bearing capacities of cast-in anchor channels. Pract Period Struct Des Constr 2016;21(4).
[11] Takase Yuya. Testing and modeling of dowel action for a post-installed anchor subjected to combined shear force and tensile force. Eng Struct 2019;195:551–8.
[12] Zhychkovska Olesya, Sheikh Shamim. Bond and anchorage behavior of alkali-silica reactive concrete. Struct J – Acids 2021;118(3):279–93 (May).
[13] Alhaidary Haidar, Al-Tamimi Adil K. Importance of performance certification for post-installed anchors: An experimental assessment. Structures 2021;29:273–85.
[14] Bolešová Mária, Gajdošová Katarína. Experimental evaluation of flat slabs strengthened with post-installed shear bolts with pre-loading. Eng Struct 2023;293:116659.
[15] Koutas L, Triantafillou TC. Use of anchors in shear strengthening of reinforced concrete T-beams with FRP. J Compos Constr 2012;17(1):101–7 (August).
[16] Philipp Mahrenholtz Richard LWood. European seismic performance categories C1 and C2 for post-installed anchors. Struct J – Acids 2020;117(6):31–44.
[17] El Menoufy Adham, Soudki Khaled. Effects of various environmental exposures and sustained load levels on the service life of postinstalled adhesive anchors. J Mater Civ Eng 2013;26(5):863–71.
[18] Mumand Fahim, Nagai Yusuke, Shigeishi Mitsuhiro. SIBIE application to detecting void at post-installed adhesive anchor in concrete. Constr Build Mater 2021;272:121916.
[19] Raza Saim, Michels Julien, Schranz Bernhard, Shahverdi Moslem. Anchorage behavior of Fe-SMA rebars Post-Installed into concrete. Eng Struct 2022;272:114960.
[20] Ahmad N. Tarawneh, Brandon E. Ross, Thomas E. Cousins Shear Behavior and Design of Post-Installed Anchors in Thin Concrete Members. Structural Journal – ACI 2020; 117(3), May: 311–322.
[21] Ghayeb Haider Hamad, Razak Hashim Abdul, Ramli Sulong NH. Performance of dowel beam-to-column connections for precast concrete systems under seismic loads: A review. Constr Build Mater 2020;237:117582.
[22] Lemcherreq Yasmin, Zanuy Carlos, Vogel Thomas, Kaufmann Walter. Strain-based analysis of reinforced concrete pull-out tests under monotonic and repeated loading. Eng Struct 2023;289:115712.
[23] Park Jun-Ryeol, Kim Sanghee, Mun Ju-Hyun, Yang Keun-Hyeok, Sim Jae-Il. Shaking table tests of veneer masonry wall retrofitted with long-rawlplug screw anchors. J Build Eng 2023;76:107163.
[24] Stehle Erik Johannes, Sharma Akanshu. Concrete cone breakout behavior of anchor groups in uncracked concrete under displacement-controlled cyclic tension load. Eng Struct 2021;246:113092.
[25] Bokor Boglárka, Sharma Akanshu, Hofmann Jan. Experimental investigations on the concrete edge failure of shear loaded anchor groups of rectangular and non-rectangular configurations. Eng Struct 2020;222:111153.
[26] Bokor Boglárka, Sharma Akanshu, Hofmann Jan (Concrete Edge Failure of Anchor Groups) Place Parallel Edge Struct J – Acids 2021;118(2):237–48.
[27] Olalusi Oladimeji B, Spyridis Panagiotis. Uncertainty modelling and analysis of the concrete edge breakout resistance of single anchors in shear. Eng Struct 2020;222:111112.
[28] Tian Kaipei, Ožbolt Joško, Hofmann Jan. Experimental investigation of concrete edge failure for single stud anchors and anchor groups after fire exposure. Constr Build Mater 2021;266:120982 (Part B).
[29] Xu Chunyi, Nehdi Moncef L, Youssef Maged A, Wang Tao, Zhang Lei V. Seismic performance of RC beam-column edge joints reinforced with austenite stainless steel. Eng Struct 2021;232:111824.
[30] Ballarini R, Yueyue X. Fracture mechanics model of anchor group breakout. J Eng Mech 2016;143(4) (November).
[31] Bokor Boglárka, Sharma Akanshu, Hofmann Jan. Experimental investigations on concrete cone failure of rectangular and non-rectangular anchor groups. Eng Struct 2019;188:202–17.
[32] Bui TT, Limam A, Nana WSA, Arrieta B, Roure T. Cast-in-place headed anchor groups under shear: experimental and numerical modelling. Structures 2018;14:178–96.
[33] Li Xing, Zhang Jiwen, Min Xinzhe, Song Shoutan, Liu Bei, Yang Yuchao, Liu Yilun. Anchorage performance of group anchored 1860-grade high-strength steel strands for beam-column connection. Constr Build Mater 2022;349:128664.
[34] Huang Baofeng, Fu Shuai, Lu Wensheng, Günay Selim. Experimental investigation of the breaking load of a dowel-pinned connection in granite cladding. Eng Struct 2020;215:110642.
[35] Pan Qiujing, Dias Daniel. Safety factor assessment of a tunnel face reinforced by horizontal dowels. Eng Struct 2017;142:56–66.
[36] Zoubek Blaž, Isakovic Tatjana, Fahjan Yasin, Fischinger Matej. Cyclic failure analysis of the beam-to-column dowel connections in precast industrial buildings. Eng Struct 2013;52:179–91.
[37] Biolzi Luigi. Mixed mode fracture in concrete beams. Eng Fract Mech 1990;35(1–3):187–93.
[38] Çalışkan Özlem, Yılmaz Salıh, Kaplan Hasan, Kıraç Nevzat. Shear strength of epoxy anchors embedded into low strength concrete. Constr Build Mater 2013;38:723–30.
[39] Piccinin Roberto, Ballarini Roberto, Cattaneo Sara. Pullout capacity of headed anchors in prestressed concrete. J Eng Mech ASCE 2012;Volume 138(7):877–87.
[40] González Francisco, Fernández Jaime, Agranati Galit, Villanueva Paula. Influence of construction conditions on strength of post installed bonded anchors. Constr Build Mater 2018;165:272–83.
[41] Meinheit DF, Heidbrink FD. Behavior of drilled-in expansion anchors. Concr Int 1985;7(4):62–6 (April).
[42] Nilforoush Rasoul, Nilsson Martin, Elfgren Lennart. Experimental evaluation of influence of member thickness, anchor-head size, and orthogonal surface reinforcement on the tensile capacity of headed anchors in uncracked concrete. J Struct Eng – ASCE 2018;144(4) (January).
[43] Odacioglu Orhan Gazi, Dogan Orhan, Kale Fulya. An experimental study to determine the optimum depth of steel anchors in RC subjected to shear force. Structures 2022;44:1321–7.
[44] J.G. Ollgaard, R.G. Slutter, J.W.Fisher. Shear strength of stud connectors in lightweight and normal weight concrete, AISC Eng'g Jr., April 1971 (71–10). Fritz Laboratory Reports 1971. Paper 2010.
[45] Ollgaard JG, Slutter RG, Shear JWFisher. Strength of stud connectors in lightweight and normal-weight concrete. Eng J 1971;Vol. 8:55–64 (American Institute of Steel Construction).
[46] K. Roik. Verbundkonstruktion (Composite construction). Stahlbau-Handbuch, Vol. 1,. Stahlbau-Verlags-GmbH, Köln, Germany: 627–672 (in German).
[47] M. Roik. Tastversuche zum Tragverhalten von senkrecht zum Rand eingebauten Ankerschienen, belastet durch. Querzug parallel zum Rand (Preliminary tests to anchor channels arranged perpendicularly to the edge and loaded by a shear load parallel to the edge). Halfen GmbH, Langenfeld, Germany, 2009 (in German).
[48] Rosca Bogdan, Serbanoiu Adrian Alexandru. Experimental study on bond performance of advanced material based on composite Portland cements developed for anchoring systems with post-installed reinforcement bars in concrete. Mater Today: Proc 2021;47:2329–36. Part 10.
[49] Shrestha Rumi, Kessler Hannah, Redmond Laura, Rangaraju Prasad. Behavior of anchor bolts in concrete masonry with lightweight grout. Struct J – Acids 2023;120(1):163–75.
[50] Ueda T, Kitipornchai S, Ling K. Experimental investigation of anchor bolts under shear. J Struct Eng – ASCE 1990;116(4):910–24.
[51] Yi Y, Kim H, Boehm RA, Webb ZD, Choi J, Murcia-Delso J, Hrynyk TD, Bayrak O. Experimental study on column reinforcing bar anchorage in drilled shaft footings. Struct J - Acids 2023;120(4):191–206.
[52] Epackachi Siamak, Esmaili Omid, Mirghaderi Seyed Rasoul, Behbahani Ali Asghar Taheri. Behavior of adhesive bonded anchors under tension and shear loads. J Constr Steel Res 2015;114:269–80.
[53] Fuchs W, Eligehausen R, Breen J. Concrete capacity design (CCD) approach for fastening to concrete. Acids Struct J 1995;92(1):73–94 (Jan.-Feb).
[54] Fuchs W, von Befestigungen Tragverhalten. unter Querlast im ungerissenen Beton (Behaviour of Fastenings under Shear Load in Uncracked Concrete). Mitteilungen 1990;No.. /2, Institut fiir Werkstoffe im Bauwesen, Universitlit Stuttgart, 1990 (in German).
[55] Gong Wenping, Martin James R, Juang CHsein, Dickenson Stephen E, McCullough Nason J. A hybrid framework for developing empirical model for seismic deformations of anchored sheetpile bulkheads. Soil Dyn Earthq Eng 2019;116:192–204.
[56] Pauletta Margherita, Di Marco Caterina, Frappa Giada, Somma Giuliana, Pitacco Igino, Miani Marco, Das Sreekanta, Russo Gaetano. Semi-empirical model for shear strength of RC interior beam-column joints subjected to cyclic loads. Eng Struct 2020;224:111223.

[57] Vita Norbert, Sharma Akanshu. Behaviour of single bonded anchors in non-cracked and cracked steel fiber reinforced concrete under short-time tensile loading. Eng Struct 2021;245:112900.
[58] El-Gendy Mohammed G, El-Salakawy Ehab F. Finite-element analysis of FRP-reinforced concrete slab-column edge connections subjected to reversed-cyclic lateral loads. J Compos Constr 2020;Volume 25(Issue 1) (November).
[59] Cortez Flores Ilsen Adriana, Fernández Gómez Jaime, Villanueva Llauradó Paula, Ferreira António, Parente Marco. Evaluation through a finite element simulation of the performance of FRP anchors for externally bonded reinforcements. Compos Struct 2021;267:113919.
[60] Gesoğlu Mehmet, Güneyisi Esra Mete, Güneyisi Erhan, Yılmaz Muhammet Enes, Mermerdaş Kasım. Modeling and analysis of the shear capacity of adhesive anchors post-installed into uncracked concrete. Compos Part B: Eng 2014;60:716–24.
[61] Jeon Siwoo, Ju Minkwan, Park Jihyuk, Choi Habeun, Park Kyoungsoo. Prediction of concrete anchor pull-out failure using cohesive zone modeling. Constr Build Mater 2023;383:130993.
[62] Shoaib Karam Muhammad, Nakamura Hikaru, Yamamoto Yoshihito, Miura Taito. Numerical evaluation of the perfobond (PBL) shear connector with transverse rebar using coupled rigid Body spring model (RBSM) and solid finite element method (FEM). Structures 2022;45:1544–60.
[63] Luo Da, Zhao Jian. Modeling crushed concrete depth and its impact on anchors shear capacities. J Struct Eng 2022;148(5) (February).
[64] Mahrenholtz Christoph, Eligehausen Rolf. Simulation of tests on cast-in and postinstalled column-to-foundation connections to quantify the effect of cyclic loading. J Struct Eng – ASCE 2015;142(1) (June).
[65] Zhao Yong, Yuan Yue, Wang Chun-Lin, Meng Shaoping. Experimental and finite element analysis of flexural performance of steel-timber composite beams connected by hybrid-anchored screws. Eng Struct 2023;292:116503.
[66] Suenaga D, Takase Y, Abe T, Orita G, Ando S. Prediction accuracy of random forest, XGBoost, LightGBM, and artificial neural network for shear resistance of post-installed anchors. Structures 2023;50:1252–63.
[67] Güneyisi EM, Gesoğlu M, Güneyisi E, et al. Assessment of shear capacity of adhesive anchors for structures using neural network based model. Mater Struct 2016;49:1065–77.
[68] Klingner RE, Tensile JA Mendonça. Capacity of short anchor bolts and welded studs: a literature review. ACI J. 1982;79(4):270–9.
[69] Corradi M, Borri A, Poverello E, Castori G. The use of transverse connectors as reinforcement of multi-leaf walls. Mater Struct/Mater Et Constr 2017;50(2):114 (art. no).
[70] Silveri F, Riva P, Profeta G, Belleri A, Poverello E, Panzeri P. San Giovanni Battista church: operational modal analysis after injected anchors strengthening. structural analysis of historical constructions: anamnesis, diagnosis, therapy. Controls - Proc 10th Int Conf Struct Anal Hist Constr, SAHC 2016:1125–32. Leuven, 13-15 September 2016, Code 179659.
[71] Silveri F, Riva P, Profeta G, Poverello E, Algeri C. Experimental study on injected anchors for the seismic retrofit of historical masonry buildings. Int J Archit Herit 2015;10(2-3):182–203.
[72] American Association State Highway and Transportation Officials Standard – AASHTO. Standard Specification for Structural Bolts, Steel, Heat Treated, 120/105 ksi Minimum Tensile Strength. A325.
[73] ACI Committee 349. Code requirements for nuclear safety related concrete structures – ACI 349–01, Farmington Hills, MI, USA, 2001; ACI 349–13, Farmington Hills, MI, USA, 2015.
[74] ACI Committee 318. Building code requirements for structural concrete and commentary – ACI 318–19. Commentary on Building Code Requirements for Structural Concrete – ACI 318R-19. Farmington Hills, MI, USA. 2019. Reapproved in 2022.
[75] ACI Committee 355. sEvaluating the Performance of Post-Installed Mechanical Anchors in Concrete. ACI 355.2–00. Farmington Hills, MI, USA, 2000; ACI 355.2–01. Farmington Hills, MI, USA, 2002.
[76] ACI Committee 355. Post-Installed Mechanical Anchors in Concrete – Qualification Requirements and Commentary. ACI CODE-355.2–22. Farmington Hills, MI, USA. First printing: September 2022.
[77] ASTM Standard E1512. Standard Test Methods for Testing Bond Performance of Bonded Anchors). 2015.
[78] ASTM F1554-07ae1. Standard Specification for Anchor Bolts, Steel. 36, 55, 105-ksi Yield Strength 2015.
[79] ASTM E488/E488M-18, Standard Test Methods for Strength of Anchors in Concrete Elements, ASTM International, West Conshohocken, PA, 2018,
[80] European Organisation For Technical Approvals – EOTA. Design of Bonded Anchors. Technical Report 029. Edition June 2007. Amended September 2010.
[81] fib. Design of anchorages in concrete: Guide to good practice. fib Bull 2011. n. 58: 280 pages.
[82] Standard Test Methods for Strength of Anchors in Concrete and Masonry Elements, ASTM E488–10, ASTM International, 2010.
[83] EN. Eur 2 – Des Concr Struct - Part 4: Des Fasten Use Concr 1992-4:2018.
[84] Mahrenholtz Philipp, Wood Richard L, Eligehausen Rolf, Hutchinson Tara C, Hoehler Matthew S. Development and validation of European guidelines for seismic qualification of post-installed anchors. Eng Struct 2017;148:497–508.
[85] Johnson Timothy P, Dowell Robert K, Silva John F. A review of code seismic demands for anchorage of nonstructural components. J Build Eng 2016;5:249–53.
[86] Lin Q, Biolzi L, Labuz JF. Opening and mixed-mode fracture initiation in a quasi-brittle material. J Eng Mech – ASCE 2013;139(2):177–87.